Disentangling Coupling Effects in the Infrared Spectra of Liquid Water

Kelly M. Hunter,* Farnaz A. Shakib, and Francesco Paesani*

Department of Chemistry and Biochemistry, University of California, San Diego

La Jolla, California 92093, United States

E-mail: k6hunter@ucsd.edu; fpaesani@ucsd.edu

Abstract

A quantitative characterization of intermolecular and intramolecular couplings that modulate the OH-stretch vibrational band in liquid water has so far remained elusive. Here, we take up this challenge by combining the centroid molecular dynamics (CMD) formalism, which accounts for nuclear quantum effects, with the MB-pol potential energy function, which accurately reproduces the properties of water across all phases, to model the infrared (IR) spectra of various isotopic water solutions with different levels of vibrational couplings, including those that cannot be probed experimentally. Analysis of the different IR OH-stretch lineshapes provides direct evidence for the partially quantum-mechanical nature of hydrogen bonds in liquid water, which is emphasized by synergistic effects associated with intermolecular coupling and many-body electrostatic interactions. Furthermore, we quantitatively demonstrate that intramolecular coupling, which results in Fermi resonances due to the mixing between HOH-bend overtones and OH-stretch fundamentals, are responsible for the shoulder located at $\sim$3250 cm^{-1} of the IR OH-stretch band of liquid water.

Introduction

Despite its apparent simplicity, with only 3 atoms and 10 electrons, water displays a unique behavior across the phase diagram which still befuddles scientists. As the most essential liquid on Earth, water exhibits several anomalous properties that are directly related to its ability to form dynamic hydrogen-bond (H-bond) networks that continually fluctuate via the breaking and forming of H-bonds. Vibrational spectroscopy is a powerful tool to investigate both structure and dynamics of the H-bond network of water in different environments.[1–4] However, an unambigous assignment of the vibrational spectra of water is highly nontrivial due to the fluctuating nature of the H-bond network and the presence of both intramolecular and intermolecular couplings.

Through selective isotopic substitutions, different types of coupling within the H-bond

network can be separated to allow for the investigation of both individual and multiple coupling effects at the same time. On the experimental side, infrared (IR) spectroscopy has been widely used to probe either fully coupled or completely isolated OH stretches of neat H_2O or diluted HOD in D_2O solutions, respectively.[5–13] However, it has proven experimentally difficult to disentangle intermediate levels of couplings due to relatively fast H/D exchange in solution that effectively precludes the monitoring of OH stretches of diluted H_2O molecules in D_2O as well as diluted HOD molecules in H_2O, which would be ideal systems for independently characterizing intramolecular and intermolecular couplings, respectively. On the other hand, the majority of theoretical studies have focused on fully coupled or isolated OH stretches in order to provide molecular interpretations of the experimental spectra.[14–33] These limitations on both experimental and theoretical sides have so far prevented a quantitative assessment of coupling effects in the structural rearrangements of the water H-bond network.

The introduction of highly accurate many-body potential energy functions (PEFs) for water, such as CC-pol,[34–36] WHBB,[37–39] HBB2-pol,[40,41] and MB-pol,[42–46] has effectively transformed the landscape of water simulations, enhancing the prospect for predictive theoretical studies of water at the molecular level. Among the existing many-body PEFs, we and others have shown that MB-pol correctly predicts the properties of water from the gas to the condensed phase, reproducing the vibration-rotation tunneling spectrum of the water dimer,[43] the energetics of small clusters,[44] the isomeric quantum equilibria and tunneling pathways of the water hexamer,[47,48] structural, thermodynamic, and dynamical properties of liquid water,[45,46] and the energetics of the ice phases.[49] MB-pol has also been shown to accurately reproduce the THz spectra of the octamer cluster,[50] the infrared and Raman spectra of liquid water,[29,32,51] the temperature-dependence of the sum-frequency generation spectra of the air/water interface,[52] and the infrared and Raman spectra of ice I_h.[53] More recently, molecular configurations extracted from classical and path-integral molecular dynamics simulations with MB-pol have been used in many-body perturbation theory calculations to

model the X-ray absorption spectrum of liquid water as well as to determine the electron affinity of water, both in the bulk and at the air/water interface.[54,55]

Building upon the demonstrated predictive power of MB-pol and taking advantage of the fact that isotope exchange is a rare event in computer simulations of water, which is completely turned off when using non-dissociable models, we present a systematic investigation of IR OH-stretch lineshapes calculated for different isotopic mixtures. Specifically, we report the results of centroid molecular dynamics (CMD) simulations for four different solutions: neat H_2O, diluted HOD in H_2O, diluted H_2O in D_2O, and diluted HOD in D_2O, corresponding to solutions with fully coupled OH stretches, only intermolecularly coupled OH stretches, only intramolecularly coupled OH stretches, and fully decoupled OH stretches, respectively. The combination of MB-pol, a water model exhibiting chemical and spectroscopic accuracy, with quantum dynamics simulations carried out within the CMD formalism allows for unambiguously disentangling intramolecular and intermolecular coupling effects on both the frequency shift and intensity of the OH-stretch lineshape in liquid water, which has so far remained elusive. Furthermore, by combining the local mode[56,57] and local monomer[39] (LM) methods, calculations carried out on molecular configurations extracted along the CMD trajectories allow for further dissecting the IR OH-stretch lineshape by quantifying contributions due to Fermi resonances.

Computational Methods

To investigate coupling effects on the vibrational dynamics of the H-bond network in liquid water, four isotopic solutions (neat H_2O, diluted HOD in H_2O, diluted H_2O in D_2O, and diluted HOD in D_2O) with different degrees of intramolecular and intermolecular couplings, as depicted in Figure 1, are investigated. Within each solution, we focus our analysis on the OH stretch vibrations; for neat H_2O, we investigate both intramolecular and intermolecular couplings (Fig. 1a), for HOD in H_2O, we specifically monitor the OH vibrations of the

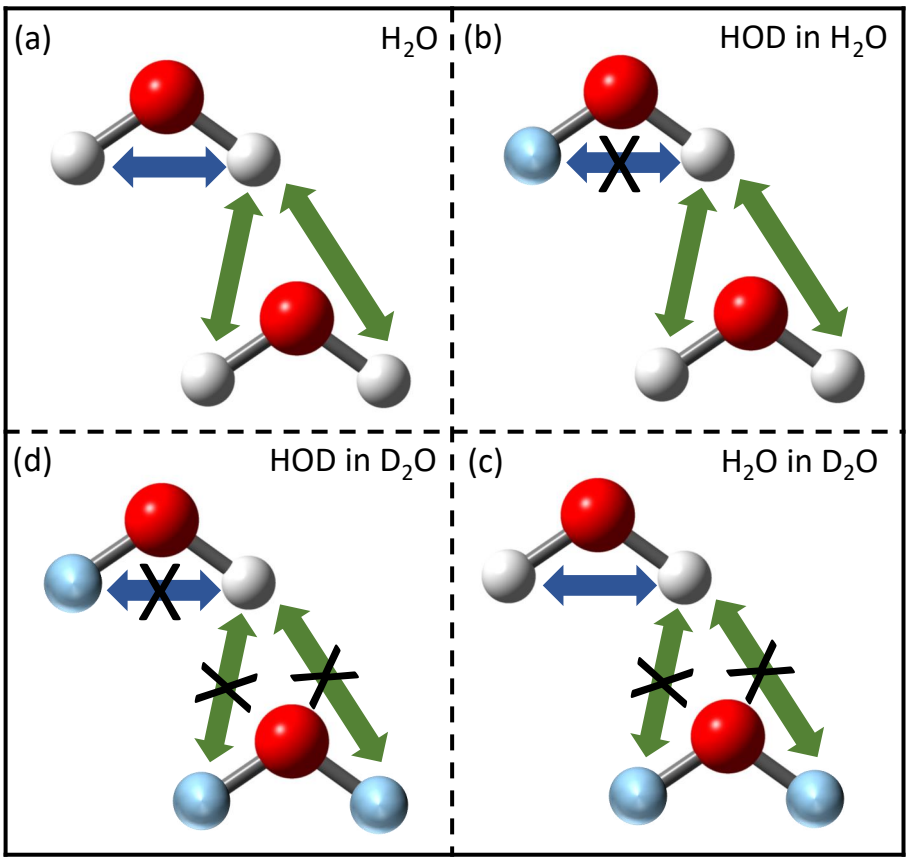

Figure 1: Depiction of the different coupling effects in the four isotopic solutions analyzed in this study. The oxygen atoms are shown in red, the hydrogen atoms in white, and the deuterium atoms in blue. The top left molecule in each panel represents the "solute" molecule being probed in the calculations of the corresponding IR OH-stretch lineshape, and the bottom right molecule is one of the "solvent" molecules. Blue arrows represent intramolecular coupling, and green arrows represent intermolecular coupling.

"solute" HOD molecules which are intermolecularly coupled to the OH vibrations of the "solvent" H_2O molecules (Fig. 1b), for H_2O in D_2O, we consider the OH stretches of the "solute" H_2O molecules which are intramolecularly coupled but completely decoupled from the OD vibrations of the solvent D_2O molecules (Fig. 1c), and for HOD in D_2O, we investigate the uncoupled OH vibrations of the "solute" HOD molecule (Fig. 1d). Analogous simulations, presented in the Supporting Information, were also performed to characterize coupling effects on the OD-stretch vibrational dynamics.

Nuclear quantum effects (NQE) are accounted for within the CMD formalism, which ap-

proximates the exact quantum expressions in terms of phase space representations amenable to classical-like interpretations of the variables of interest.[58–62] In all CMD simulations, each atom is represented by a Feynman's ring-polymer discretized with 32 beads, and the centroid variables are propagated according to the velocity-Verlet algorithm using the partially adiabatic separation scheme of Refs. 61 and 63, with an adiabaticity parameter $\gamma = 0.25$ and a time step of 0.05 fs. A Nosé-Hoover chain of four thermostats is attached to each degree of freedom to ensure adequate canonical sampling at 298.15 K. Short-range interactions are truncated at an atom-atom separation of 9.0 Å, while the electrostatic interactions are treated using the Ewald sum.[64] Each isotopic solution consists of 216 molecules total, with two "solute" molecules surrounded by 214 "solvent" molecules (e.g. two HOD molecules in 214 D_2O molecules) to mimic the 1% concentration typically used in experiments.[3] 20 independent CMD trajectories are collected for each isotopic solution, starting from initial configurations extracted from previous path-integral molecular dynamics (PIMD) simulations carried out for H_2O and D_2O solutions at the corresponding experimental densities.[32,51] Cubic simulation boxes with sides of 18.6428 Å and 18.6506 Å are thus used for isotopic mixtures with H_2O and D_2O as the "solvents", respectively.

In all simulations, the water interactions are described by MB-pol, a many-body PEF rigorously derived from the many-body expansion of the interaction energy between water molecules,[43–45] which has been shown to provide an accurate representation of water across different phases.[46] The IR spectra for all isotopic solutions are calculated within the time-dependent formalism according to

$$I_{IR}(\omega) = \Big[\frac{2\omega}{3V\hbar c\epsilon_0}\Big] \tanh(\beta\hbar\omega) \int_{-\infty}^{\infty} dt\, e^{i\omega t} \langle \mu(0)\mu(t)\rangle \tag{1}$$

where V is the system volume, c is the speed of light, ϵ_0 is the permittivity of free space, and $\beta = (k_B T)^{-1}$, with k_B being Boltzmann's constant. In Eq. 1, $\langle \mu(0)\mu(t)\rangle$ is the ensemble averaged quantum dipole-dipole time correlation function obtained for each isotopic solution

by averaging $\mu(0)\mu(t)$ over the corresponding 20 independent CMD trajectories, with $\mu(t)$ given by the many-body MB-μ function introduced in Ref. 29. MB-μ includes explicit one-body (1B) and two-body (2B) terms, with all higher-order N-body (NB) terms being described by classical induction.

Finally, to quantify Fermi resonance contributions deemed to be important to the H_2O IR lineshape,[65] local mode and local monomer (LM) calculations[39,56,57] are performed on molecular clusters consisting of 16 D_2O molecules around a H_2O molecule, which were extracted from the corresponding CMD simulations carried out for the diluted H_2O in D_2O solution. In the LM calculations, the coordinates of the D_2O molecules as well as the oxygen atom of the H_2O molecule are kept fixed to their CMD values, while constrained optimizations of the hydrogen positions are performed by interfacing the ORCA package[66] with our in-house MB-pol software.

Results and Discussion

To first assess the accuracy of our theoretical and computational approach, the IR lineshapes calculated from CMD simulations of neat H_2O and diluted HOD in D_2O solutions are compared with the corresponding experimental spectra in Figure 2. Similar comparisons were reported in different contexts in previous studies with MB-pol.[29,32] As discussed in detail in Refs. 29 and 32, MB-pol slightly underestimates the H-bond strength in liquid water, which results in OH stretching frequencies that are approximately 57 cm^{-1} blue-shifted compared to experiment. After accounting for this shift, overall good agreement is found between the theoretical and experimental lineshapes, which is nearly quantitative for the HOD in D_2O system. However, some noticeable differences exist in the low-frequency region of the neat H_2O lineshape with the CMD band lacking intensity between 3000 cm^{-1} and 3300 cm^{-1}, as originally observed in Ref. 29.

The IR lineshapes calculated for the "solute" molecules (i.e., H_2O or HOD) of the four

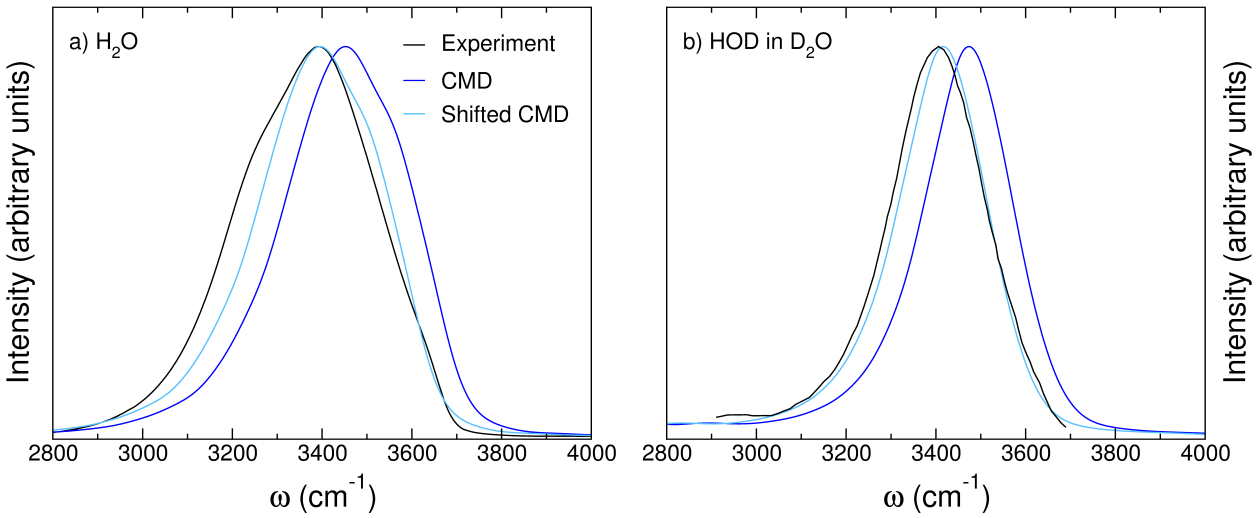

Figure 2: IR OH-stretch lineshapes (blue traces) calculated from CMD simulations of neat H_2O (a) and diluted HOD in D_2O (b) solutions compared with the corresponding experimental results (black traces) from Refs.[5] and 7, respectively. Also shown are the CMD lineshapes (light blue) red-shifted by 57 cm^{-1} to facilitate comparisons with the experimental results. See main text for details.

different isotopic solutions are shown in Fig. 3. To further characterize the interplay between vibrational and electrostatic couplings, the IR lineshapes for each isotopic solution are calculated using different representations of the dipole moment in Eq. 1, corresponding to different approximations to many-body effects on the water dipole moment within the MB-μ expression.[29] Specifically, each panel of Fig. 3 shows comparisons between IR lineshapes computed using the gas-phase (1B) term (red traces), the 1B+NB representation including many-body effects through classical induction (green traces), and the full many-body (1B+2B+NB) MB-μ representation which, in addition to inductive many-body effects, accounts for explicit short-range 2B contributions (blue traces). In this analysis, all lineshapes are normalized with respect to the number of OH oscillators of the "solute" molecules to allow for comparisons of both frequency shifts and intensities as a function of different levels of coupling. The full-width at half maximum (fwhm) and frequency of maximum absorbance (fma) are calculated and compared among different approximations to the many-body dipole moment in Table 1. The fwhm for neat H_2O and HOD in D_2O calculated with the 1B+2B+NB representation of the dipole moment are 337 cm^{-1} and 237

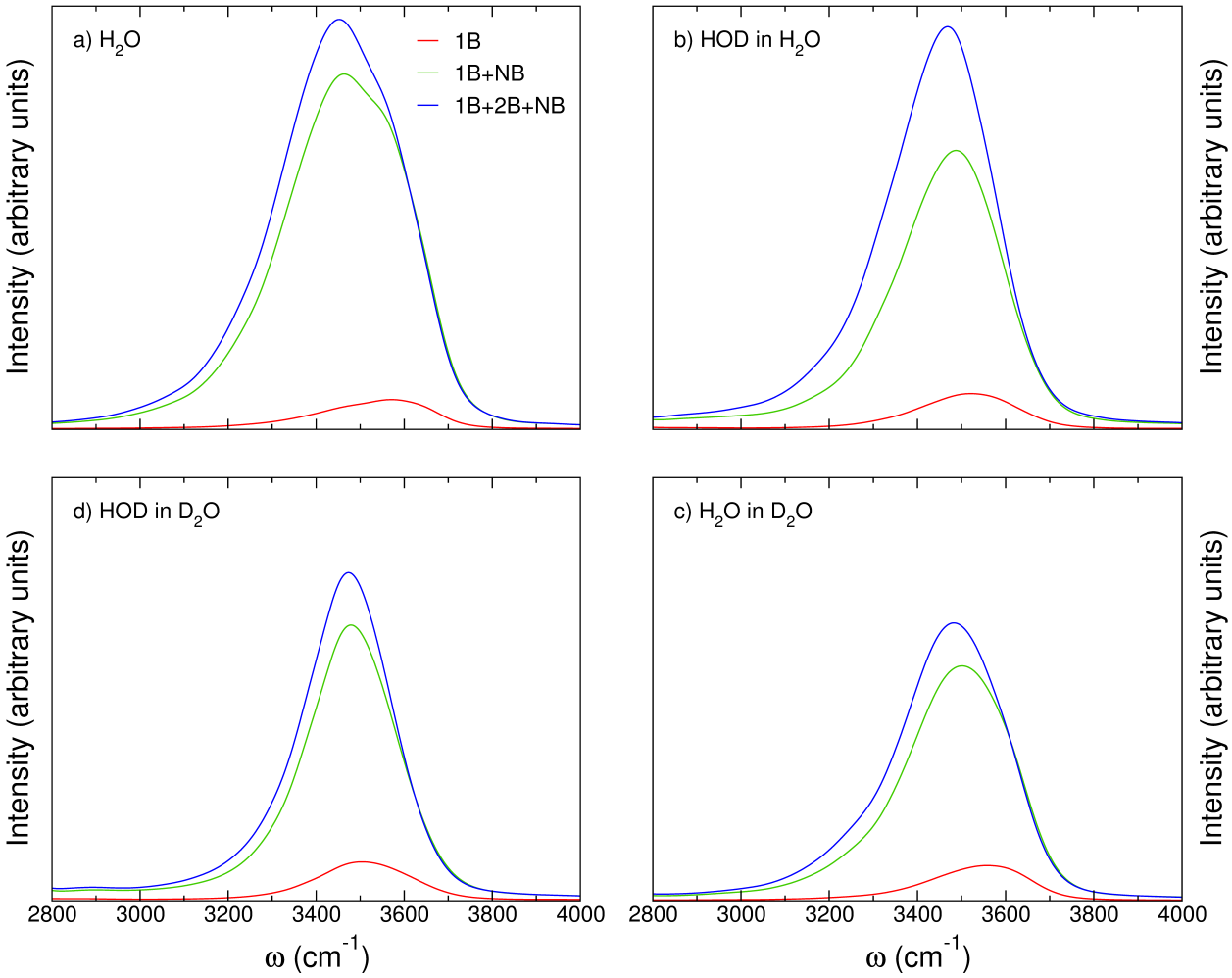

Figure 3: IR OH-stretch lineshapes calculated from CMD simulations of neat H_2O (a), diluted HOD in H_2O (b), diluted H_2O in D_2O (c), and diluted HOD in D_2O (d). For each isotopic solution, the OH-stretch lineshape is calculated using the 1B, 1B+NB, and 1B+2B+NB hierarchy of approximations to the dipole moment (see main text for details). All lineshapes are on the same intensity scale and are normalized to the number of OH oscillators of the "solute" molecule.

cm^{-1}, respectively, which are in good agreement with the corresponding experimental values of 378 cm^{-1} and 255 cm^{-1}.[5,7]

Fig. 3 shows that, at the 1B level of electrostatic coupling (red traces), the IR lineshapes calculated for "solutes" with intramolecular coupling (i.e., neat H_2O and H_2O in D_2O) are the most blue-shifted. As discussed in Ref. 32, due to the lack of electrostatic coupling with the surrounding "solvent" molecules, these 1B lineshapes only report on "solute" dipole moment fluctuations associated with intramolecular distortions. Since changes in the 1B

Table 1: Full-width at half maximum (fwhm) and frequency of maximum absorbance (fma) in cm^{-1} of the OH-stretch lineshape calculated for the four different isotopic solutions using the 1B, 1B+NB, and 1B+2B+NB hierarchy of approximations to the dipole moment (see main text for details).

	1B		1B+NB		1B+2B+NB	
	fwhm	fma	fwhm	fma	fwhm	fma
H_2O	294	3570	344	3463	337	3453
HOD in H_2O	260	3520	273	3486	281	3470
H_2O in D_2O	259	3560	287	3500	287	3483
HOD in D_2O	252	3503	239	3480	237	3473

(gas-phase) dipole moment due to stretching and bending vibrations in solution are relatively smaller than those associated with induction interactions,[32] the transition dipole moment remains approximately constant, independently of the instantaneous "solute" configuration. This makes the 1B lineshapes effectively identical to the corresponding lineshapes calculated within the Condon approximation using the full many-body representation of the dipole moment.[32] The blue shifts observed in the 1B lineshapes of neat H_2O and H_2O in D_2O thus indicate that intermolecular coupling is responsible for slightly stronger H-bonds and, consequently, weaker OH bonds.

Inclusion of N-body electrostatic effects (green traces) results in an overall increase in intensity of all lineshapes. Specifically, the lineshape for the fully coupled neat H_2O solution exhibits the highest intensity, while the lowest intensity is found for the lineshape of the intramolecularly coupled H_2O in D_2O solution. The lineshapes for the intermolecularly coupled HOD in H_2O and fully decoupled HOD in D_2O solutions display nearly identical intensities. Comparisons with the corresponding 1B lineshapes demonstrate that N-body electrostatic effects are clearly responsible for significant redistribution of the IR intensity over the entire frequency range of the OH vibrations, resulting in changes to the lineshapes which directly correlate with the specific level of vibrational coupling present in each solution. In particular, the 1B+NB lineshapes of both solutions with intermolecular coupling (i.e., neat H_2O and HOD in H_2O) display relatively higher intensities between 3250 cm^{-1} and 3400 cm^{-1} (see Supporting Information for specific details). Since this frequency range is

associated with stronger H-bonds, these results thus emphasize the importance of many-body electrostatic effects in the vibrational dynamics of strongly coupled OH stretches in liquid water. On the other hand, it should be noted that the lineshape of the intramolecularly coupled H_2O in D_2O solution grows in intensity below 3250 cm^{-1}.

When the dipole moments in Eq. 1 are represented by the full many-body MB-μ function, which includes a short-range 2B term in addition to a classical representation of many-body effects, further increase in the IR intensity is observed for the corresponding lineshapes (blue traces) shown in Fig. 3, particularly in the low-frequency region. The comparison among IR lineshapes calculated as a function of the level of electrostatic coupling (Table 1) shows that the fwhm calculated for the diluted HOD in H_2O, diluted H_2O in D_2O, and neat H_2O solutions increase by 21 cm^{-1}, 28 cm^{-1}, and 43 cm^{-1}, respectively, going from the 1B to the 1B+2B+NB representation of the dipole moment, while the fwhm calculated for the diluted HOD in D_2O decreases by 15 cm^{-1}. Since the 1B lineshape depends only on the gas-phase dipole moment of the HOD molecule, the narrowing of the linewidth with the increase of electrostatic coupling demonstrates that, when integrated in the H-bond network, the dipole moment of a fully decoupled OH oscillator samples a narrower distribution of values than in the gas phase. Table 1 shows that, independently of the isotopic solution, the changes in linewidths are accompanied by red shifts in the frequencies of maximum absorbance on the order of 50 cm^{-1} going from the 1B to the 1B+2B+NB representation of the dipole moment.

These changes are particularly pronounced in the lineshape of diluted HOD in H_2O. While this isotopic mixture cannot be probed in experiments, the theoretical predictions shown in Fig. 3b can be used to characterize the nature of intermolecular coupling, isolated from any other competing effects. Since, as discussed in detail in Ref. 31, the 2B term of the MB-μ function recovers electrostatic contributions associated with quantum-mechanical effects (e.g., charge transfer and penetration, and Pauli repulsion) that cannot be described by classical expressions, the large difference in IR intensity between 1B+NB and 1B+2B+NB lineshapes of diluted HOD in H_2O provides direct evidence for the par-

tially quantum-mechanical nature of H-bonds in liquid water. The 1B+2B+NB lineshape for the diluted H_2O in D_2O solution also exhibits higher intensity than its 1B+NB analog in the low-frequency region, although the differences are not as large as those observed for the diluted HOD in H_2O solution. While these results provide further support for the partially quantum-mechanical nature of H-bonds in liquid water, the differences between the lineshapes for diluted H_2O in D_2O and diluted HOD in H_2O solutions clearly indicate that 2B quantum-mechanical effects in H-bonding are enhanced by intermolecular coupling.

The analysis of the IR lineshapes for the diluted H_2O in D_2O solution (Fig. 3c), which cannot be probed experimentally, provides the unique opportunity to isolate the contributions due to intramolecular coupling. As mentioned above, compared to the lineshapes for both fully decoupled HOD in D_2O and intermolecularly coupled HOD in H_2O solutions, the lineshape for the intramolecularly coupled H_2O in D_2O solution grows in intensity below 3250 cm^{-1}. To determine the origin of this intensity enhancement, we performed LM calculations.[39,56,57] Since, by construction, the LM method provides a rigorous theoretical framework for identifying both fundamental and overtone transitions, it allows for the dissection of the OH lineshape in terms of actual OH stretching vibrations and HOH bending overtones, which may give rise to Fermi resonances.[27,30,65] However, due to the associated computational cost, LM calculations are only carried out on clusters consisting of a H_2O molecule solvated by 16 D_2O molecules, which are extracted from the CMD trajectories for the diluted H_2O in D_2O solution. The LM results, decomposed in contributions associated with HOH bending overtones (red) and OH stretching vibrations (blue) are shown along with the corresponding 1B+2B+NB (dashed) lineshape in Fig. 4a. Also shown for reference are both experimental (solid black) and CMD (dashed) lineshapes for neat H_2O. The comparison between LM and CMD results indicates that the relative increase in intensity observed below 3250 cm^{-1} in the 1B+2B+NB lineshape for the diluted H_2O in D_2O solution can be attributed to Fermi resonances arising from quantum-mechanical mixing between HOH bending overtones and OH stretching fundamentals as recently suggested.[29,30,32,33,65]

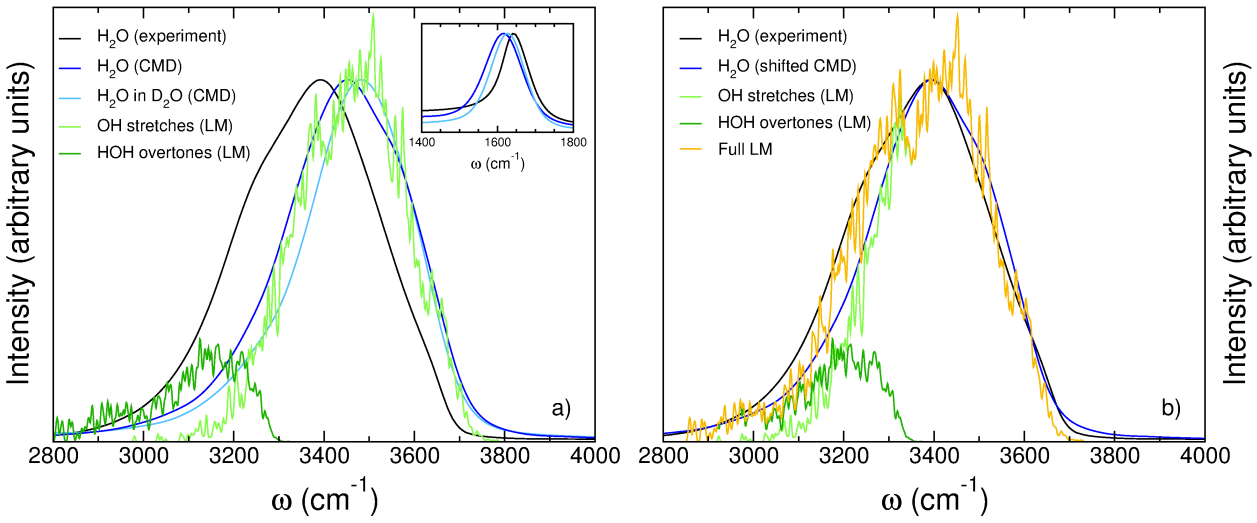

Figure 4: a) LM frequency distributions of OH stretches (light green) and HOH-bend overtones (dark green) calculated for diluted H_2O in D_2O, experimental (black) and CMD (blue) IR OH-stretch lineshapes of neat H_2O, and CMD (light blue) IR OH-stretch lineshape of diluted H_2O in D_2O. b) LM frequency distributions of OH stretches (light green) and HOH-bend overtones (dark green) calculated for diluted H_2O in D_2O and shifted by -57 cm^{-1} and 50 cm^{-1}, respectively, full LM lineshape (yellow), experimental (black) and CMD (blue) IR OH-stretch lineshapes of neat H_2O, with the latter being shifted by -57 cm^{-1}. See main text for details.

This analysis also sheds light on the missing intensity in the low-frequency region of the CMD IR lineshape for the neat H_2O solution compared to experiment. As mentioned above and discussed in detail in Refs. 29 and 32, MB-pol slightly underestimates the strength of H-bonds in liquid water, which translates into a 57 cm^{-1} blue shift of the calculated OH stretch lineshape relative to experiment. At the same time, weaker H-bonds also lead to a $\sim$25 cm^{-1} red shift of the calculated HOH bend lineshape (see inset in Fig. 4a). After correcting for these inaccuracies by shifting the LM OH-stretch and HOH-bend-overtone frequency distributions by -57 cm^{-1} and 50 cm^{-1} (twice the difference from the bending region), respectively, Figure 4b shows that the lineshape obtained by adding the two LM components is in excellent agreement with the experimental lineshape, recovering, almost completely, the missing intensity below $\sim$3300 cm^{-1}. The results reported in Fig. 4b thus demonstrate that the differences between the CMD and experimental OH-stretch lineshapes can be traced back to MB-pol slightly underestimating the strength of H-bonds in liquid

water which, in turn, results in the underestimation of Fermi resonance contributions due to the predicted weaker coupling between OH stretches and HOH bend overtones. In this regard, it should be noted that a deviation of 57 cm^{-1}, corresponding to 0.16 kcal/mol, is well within what is currently defined chemical accuracy (1 kcal/mol), which is achieved by MB-pol. This implies that, as originally suggested in Ref. 29, a quantitative representation of the IR OH-stretch lineshape might effectively require "exact" knowledge of the multidimensional Born-Oppenheimer potential energy surface of liquid water, including an accurate description of autoionization, which is currently beyond reach of even the most sophisticated electronic structure methods.

Conclusions

In this study, we have combined accurate modeling of water through the use of the MB-pol potential energy function with CMD simulations that account for nuclear quantum effects. Building upon our previous studies,[29,32] we have investigated four isotopic solutions with different levels of vibrational coupling, including neat H_2O, diluted HOD in H_2O, diluted H_2O in D_2O, and diluted HOD in D_2O solutions. Our analysis, carried out with different approximations to many-body effects in the representation of the water dipole moment, indicates that the IR OH-stretch lineshapes of all four isotopic solutions increase in intensity and shift toward lower frequencies as electrostatic couplings are taken into account. In this regard, the narrowing of the lineshape for the diluted HOD in D_2O solution going from the 1B to the 1B+2B+NB representation of the dipole moment demonstrates that the dipole moment of a fully decoupled OH oscillator immersed in the D_2O H-bond network samples a narrower distribution than in the gas phase.

Comparisons between the IR OH-stretch lineshapes for the diluted HOD in H_2O and diluted H_2O in D_2O solutions, which cannot be probed experimentally due to isotope exchange, have allowed us to further disentangle the IR OH-stretch lineshape of neat H_2O into

effects associated with intermolecular and intramolecular couplings. In particular, the analysis of the IR lineshape of the intermolecularly coupled OH stretch of HOD in H_2O provides direct evidence for the partially quantum-mechanical nature of H-bonds in liquid water, with intermolecular coupling becoming larger for stronger H-bonds. On the other hand, the IR lineshape of the intramolecularly coupled OH stretch of H_2O in D_2O shows the presence of significant overlap between the frequencies of the IR OH-stretch fundamentals and HOH-bend overtones. Additional LM calculations carried out for the OH stretches of H_2O in D_2O have allowed us to quantify the role played by Fermi resonances in modulating the IR OH-stretch lineshape. In particular, by taking into account that MB-pol slightly underestimates the H-bond strength in liquid water, the present results quantitatively demonstrate that Fermi resonances are responsible for the shoulder at $\sim$3250 cm^{-1} of the IR OH-stretch lineshape of neat H_2O.

Supporting Information

Additional comparisons of the IR OH-stretch lineshapes along with the analogous IR OD-stretch lineshapes are presented. It is shown that similar conclusions about the role of intramolecular and intermolecular couplings can be drawn from the analysis of the IR OD-stretch lineshapes.

Acknowledgments

This research was supported by the National Science Foundation through grant no. CHE-1453204 and used resources of the Extreme Science and Engineering Discovery Environment (XSEDE),[67] which is supported by the National Science Foundation through grant no. ACI-1053575, under allocation TG-CHE110009 as well as computational resources of the Air Force Office of Scientific Research through grant no. FA9550-16-1-0327.

References

(1) Rey, R.; Møller, K. B.; Hynes, J. T. Ultrafast Vibrational Population Dynamics of Water and Related Systems: A Theoretical Perspective. *Chem. Rev.* **2004**, *104*, 1915–1928.

(2) Paesani, F.; Voth, G. A. The Properties of Water: Insights from Quantum Simulations. *J. Phys. Chem. B* **2009**, *113*, 5702–5719.

(3) Bakker, H. J.; Skinner, J. L. Vibrational Spectroscopy as a Probe of Structure and Dynamics in Liquid Water. *Chem. Rev.* **2010**, *110*, 1498–1517.

(4) Perakis, F.; De Marco, L.; Shalit, A.; Tang, F.; Kann, Z. R.; Khne, T. D.; Torre, R.; Bonn, M.; Nagata, Y. Vibrational Spectroscopy and Dynamics of Water. *Chem. Rev.* **2016**, *116*, 7590–7607.

(5) Bertie, J. E.; Lan, Z. Infrared Intensities of Liquids XX: The Intensity of the OH Stretching Band of Liquid Water Revisited, and the Best Current Values of the Optical Constants of H_2O(l) at 25°C between 15,000 and 1 cm^{-1}. *Appl. Spectrosc.* **1996**, *50*, 1047–1057.

(6) Fecko, C. J.; Eaves, J. D.; Loparo, J. J.; Tokmakoff, A.; Geissler, P. L. Ultrafast Hydrogen-Bond Dynamics in the Infrared Spectroscopy of Water. *Science* **2003**, *301*, 1698–1702.

(7) Fecko, C. J.; Loparo, J. J.; Roberts, S. T.; Tokmakoff, A. Local Hydrogen Bonding Dynamics and Collective Reorganization in Water: Ultrafast Infrared Spectroscopy of HOD/D_2O. *J. Chem. Phys.* **2005**, *122*, 054506.

(8) Asbury, J. B.; Steinel, T.; Stromberg, C.; Corcelli, S. A.; Lawrence, C. P.; Skinner, J. L.; Fayer, M. D. Water Dynamics: Vibrational Echo Correlation Spectroscopy and Comparison to Molecular Dynamics Simulations. *J. Phys. Chem. A* **2004**, *108*, 1107–1119.

(9) Loparo, J. J.; Roberts, S. T.; Nicodemus, R. A.; Tokmakoff, A. Variation of the Transition Dipole Moment Across the OH Stretching Band of Water. *Chem. Phys.* **2007**, *341*, 218 – 229.

(10) Nicodemus, R. A.; Corcelli, S. A.; Skinner, J. L.; Tokmakoff, A. Collective Hydrogen Bond Reorganization in Water Studied with Temperature-Dependent Ultrafast Infrared Spectroscopy. *J. Phys. Chem. B* **2011**, *115*, 5604–5616.

(11) Ramasesha, K.; De Marco, L.; Mandal, A.; Tokmakoff, A. Water Vibrations Have Strongly Mixed Intra- and Intermolecular Character. *Nat. Chem.* **2013**, *5*, 935–940.

(12) De Marco, L.; Ramasesha, K.; Tokmakoff, A. Experimental Evidence of Fermi Resonances in Isotopically Dilute Water from Ultrafast Broadband IR Spectroscopy. *J. Phys. Chem. B* **2013**, *117*, 15319–15327.

(13) De Marco, L.; Carpenter, W.; Liu, H.; Biswas, R.; Bowman, J. M.; Tokmakoff, A. Differences in the Vibrational Dynamics of H_2O and D_2O: Observation of Symmetric and Antisymmetric Stretching Vibrations in Heavy Water. *J. Phys. Chem. Lett.* **2016**, *7*, 1769–1774.

(14) Rey, R.; Møller, K. B.; Hynes, J. T. Hydrogen Bond Dynamics in Water and Ultrafast Infrared Spectroscopy. *J. Phys. Chem. A* **2002**, *106*, 11993–11996.

(15) Lawrence, C. P.; Skinner, J. L. Vibrational Spectroscopy of HOD in Liquid D_2O. I. Vibrational Energy Relaxation. *J. Chem. Phys.* **2002**, *117*, 5827–5838.

(16) Lawrence, C. P.; Skinner, J. L. Vibrational Spectroscopy of HOD in Liquid D_2O. II. Infrared Line Shapes and Vibrational Stokes Shift. *J. Chem. Phys.* **2002**, *117*, 8847–8854.

(17) Lawrence, C. P.; Skinner, J. L. Vibrational Spectroscopy of HOD in Liquid D_2O. III.

Spectral Diffusion, and Hydrogen-Bonding and Rotational Dynamics. *J. Chem. Phys.* **2003**, *118*, 264–272.

(18) Lawrence, C. P.; Skinner, J. L. Vibrational Spectroscopy of HOD in Liquid D_2O. VI. Intramolecular and Intermolecular Vibrational Energy Flow. *J. Chem. Phys.* **2003**, *119*, 1623–1633.

(19) Møller, K. B.; Rey, R.; Hynes, J. T. Hydrogen Bond Dynamics in Water and Ultrafast Infrared Spectroscopy: A Theoretical Study. *J. Phys. Chem. A* **2004**, *108*, 1275–1289.

(20) Corcelli, S. A.; Lawrence, C. P.; Skinner, J. L. Combined Electronic Structure/Molecular Dynamics Approach for Ultrafast Infrared Spectroscopy of Dilute HOD in Liquid H_2O and D_2O. *J. Chem. Phys.* **2004**, *120*, 8107–8117.

(21) Corcelli, S. A.; Skinner, J. L. Infrared and Raman Line Shapes of Dilute HOD in Liquid H_2O and D_2O from 10 to 90 C. *J. Phys. Chem. A* **2005**, *109*, 6154–6165.

(22) Auer, B. M.; Skinner, J. L. IR and Raman Spectra of Liquid Water: Theory and Interpretation. *J. Chem. Phys.* **2008**, *128*, 224511.

(23) Auer, B.; Skinner, J. Water: Hydrogen Bonding and Vibrational Spectroscopy, in the Bulk Liquid and at the Liquid/Vapor Interface. *Chem. Phys. Lett.* **2009**, *470*, 13 – 20.

(24) Paesani, F.; Xantheas, S. S.; Voth, G. A. Infrared Spectroscopy and Hydrogen-Bond Dynamics of Liquid Water from Centroid Molecular Dynamics with an Ab Initio-Based Force Field. *J. Phys. Chem. B* **2009**, *113*, 13118–13130.

(25) Yang, M.; Skinner, J. L. Signatures of Coherent Vibrational Energy Transfer in IR and Raman Line Shapes for Liquid Water. *Phys. Chem. Chem. Phys.* **2010**, *12*, 982–991.

(26) Shi, L.; Gruenbaum, S. M.; Skinner, J. L. Interpretation of IR and Raman Line Shapes for H_2O and D_2O Ice Ih. *J. Phys. Chem. B* **2012**, *116*, 13821–13830.

(27) Wang, Y.; Bowman, J. M. IR Spectra of the Water Hexamer: Theory, with Inclusion of the Monomer Bend Overtone, and Experiment Are in Agreement. *J. Phys. Chem. Lett.* **2013**, *4*, 1104–1108.

(28) Ni, Y.; Skinner, J. L. IR and SFG Vibrational Spectroscopy of the Water Bend in the Bulk Liquid and at the Liquid-Vapor Interface, Respectively. *J. Chem. Phys.* **2015**, *143*, 014502.

(29) Medders, G. R.; Paesani, F. Infrared and Raman Spectroscopy of Liquid Water through First-Principles Many-Body Molecular Dynamics. *J. Chem. Theory Comput.* **2015**, *11*, 1145–1154.

(30) Liu, H.; Wang, Y.; Bowman, J. M. Quantum Calculations of the IR Spectrum of Liquid Water Using Ab Initio and Model Potential and Dipole Moment Surfaces and Comparison with Experiment. *J. Chem. Phys.* **2015**, *142*, 194502.

(31) Medders, G. R.; Paesani, F. On the Interplay of the Potential Energy and Dipole Moment Surfaces in Controlling the Infrared Activity of Liquid Water. *J. Chem. Phys.* **2015**, *142*, 212411.

(32) Straight, S. C.; Paesani, F. Exploring Electrostatic Effects on the Hydrogen Bond Network of Liquid Water through Many-Body Molecular Dynamics. *J. Phys. Chem. B* **2016**, *120*, 8539–8546.

(33) Liu, H.; Wang, Y.; Bowman, J. M. Transferable ab Initio Dipole Moment for Water: Three Applications to Bulk Water. *J. Phys. Chem. B* **2016**, *120*, 1735–1742.

(34) Bukowski, R.; Szalewicz, K.; Groenenboom, G. C.; van der Avoird, A. Predictions of the Properties of Water from First Principles. *Science* **2007**, *315*, 1249–1252.

(35) Bukowski, R.; Szalewicz, K.; Groenenboom, G. C.; van der Avoird, A. Polarizable

Interaction Potential for Water from Coupled Cluster Calculations. I. Analysis of Dimer Potential Energy Surface. *J. Chem. Phys.* **2008**, *128*, 094313.

(36) Bukowski, R.; Szalewicz, K.; Groenenboom, G. C.; van der Avoird, A. Polarizable Interaction Potential for Water from Coupled Cluster Calculations. II. Applications to Dimer Sspectra, Virial Coefficients, and Simulations of Liquid Water. *J. Chem. Phys.* **2008**, *128*, 094314.

(37) Wang, Y.; Shepler, B. C.; Braams, B. J.; Bowman, J. M. Full-Dimensional, Ab Initio Potential Energy and Dipole Moment Surfaces for Water. *J. Chem. Phys.* **2009**, *131*, 054511.

(38) Wang, Y.; Huang, X.; Shepler, B. C.; Braams, B. J.; Bowman, J. M. Flexible, Ab Initio Potential, and Dipole Moment Surfaces for Water. I. Tests and Applications for Clusters up to the 22-mer. *J. Chem. Phys.* **2011**, *134*, 094509.

(39) Wang, Y.; Bowman, J. M. Ab Initio Potential and Dipole Moment Surfaces for Water. II. Local-Monomer Calculations of the Infrared Spectra of Water Clusters. *J. Chem. Phys.* **2011**, *134*, 154510.

(40) Babin, V.; Medders, G. R.; Paesani, F. Toward a Universal Water Model: First Principles Simulations from the Dimer to the Liquid Phase. *J. Phys. Chem. Lett.* **2012**, *3*, 3765–3769.

(41) Medders, G. R.; Babin, V.; Paesani, F. A Critical Assessment of Two-Body and Three-Body Interactions in Water. *J. Chem. Theory Comput.* **2013**, *9*, 1103–1114.

(42) Medders, G. R.; Paesani, F. Many-Body Convergence of the Electrostatic Properties of Water. *J. Chem. Theory Comput.* **2013**, *9*, 4844–4852.

(43) Babin, V.; Leforestier, C.; Paesani, F. Development of a "First Principles" Water Po-

tential with Flexible Monomers: Dimer Potential Energy Surface, VRT Spectrum, and Second Virial Coefficient. *J. Chem. Theory Comput.* **2013**, *9*, 5395–5403.

(44) Babin, V.; Medders, G. R.; Paesani, F. Development of a "First Principles" Water Potential with Flexible Monomers. II: Trimer Potential Energy Surface, Third Virial Coefficient, and Small Clusters. *J. Chem. Theory Comput.* **2014**, *10*, 1599–1607.

(45) Medders, G. R.; Babin, V.; Paesani, F. Development of a "First-Principles" Water Potential with Flexible Monomers. III. Liquid Phase Properties. *J. Chem. Theory Comput.* **2014**, *10*, 2906–2910.

(46) Reddy, S. K.; Straight, S. C.; Bajaj, P.; Huy Pham, C.; Riera, M.; Moberg, D. R.; Morales, M. A.; Knight, C.; Gtz, A. W.; Paesani, F. On the Accuracy of the MB-pol Many-Body Potential for Water: Interaction Energies, Vibrational Frequencies, and Classical Thermodynamic and Dynamical Properties from Clusters to Liquid Water and Ice. *J. Chem. Phys.* **2016**, *145*, 194504.

(47) Richardson, J. O.; Pérez, C.; Lobsiger, S.; Reid, A. A.; Temelso, B.; Shields, G. C.; Kisiel, Z.; Wales, D. J.; Pate, B. H.; Althorpe, S. C. Concerted Hydrogen-Bond Breaking by Quantum Tunneling in the Water Hexamer Prism. *Science* **2016**, *351*, 1310–1313.

(48) Brown, S. E.; Gtz, A. W.; Cheng, X.; Steele, R. P.; Mandelshtam, V. A.; Paesani, F. Monitoring Water Clusters "Melt" Through Vibrational Spectroscopy. *J. Am. Chem. Soc.* **2017**, *139*, 7082–7088.

(49) Pham, C. H.; Reddy, S. K.; Chen, K.; Knight, C.; Paesani, F. Many-Body Interactions in Ice. *J. Chem. Theory Comput.* **2017**, *13*, 1778–1784.

(50) Cole, W. T. S.; Farrell, J. D.; Wales, D. J.; Saykally, R. J. Structure and Torsional Dynamics of the Water Octamer from THz Laser Spectroscopy Near 215 μm. *Science* **2016**, *352*, 1194–1197.

(51) Reddy, S. K.; Moberg, D. R.; Straight, S. C.; Paesani, F. Temperature-Dependent Vibrational Spectra and Structure of Liquid Water from Classical and Quantum Simulations with the MB-pol Potential Energy Function. *J. Chem. Phys.* **2017**, *147*, 244504.

(52) Moberg, D. R.; Straight, S. C.; Paesani, F. Temperature Dependence of the Air/Water Interface Revealed by Polarization Sensitive Sum-Frequency Generation Spectroscopy. *J. Phys. Chem. B* **2018**, *122*, 4356–4365.

(53) Moberg, D. R.; Straight, S. C.; Knight, C.; Paesani, F. Molecular Origin of the Vibrational Structure of Ice Ih. *J. Phys. Chem. Lett.* **2017**, *8*, 2579–2583, PMID: 28541703.

(54) Sun, Z.; Zheng, L.; Chen, M.; Klein, M. L.; Paesani, F.; Wu, X. Electron-Hole Theory of the Effect of Quantum Nuclei on the X-ray Absorption Spectra of Liquid Water. *Phys. Rev. Lett.* **2018**, *121*, 137401.

(55) Gaiduk, A. P.; Pham, T. A.; Govoni, M.; Paesani, F.; Galli, G. Electron Affinity of Liquid Water. *Nat. Commun.* **2018**, *9*, 247.

(56) Cheng, X.; Steele, R. P. Efficient Anharmonic Vibrational Spectroscopy for Large Molecules Using Local-Mode Coordinates. *J. Chem. Phys.* **2014**, *141*, 104105.

(57) Cheng, X.; Talbot, J. J.; Steele, R. P. Tuning Vibrational Mode Localization with Frequency Windowing. *J. Chem. Phys.* **2016**, *145*, 124112.

(58) Cao, J.; Voth, G. A. The Formulation of Quantum Statistical Mechanics Based on the Feynman Path Centroid Density. I. Equilibrium Properties. *J. Chem. Phys.* **1994**, *100*, 5093–5105.

(59) Cao, J.; Voth, G. A. The Formulation of Quantum Statistical Mechanics Based on the Feynman Path Centroid Density. II. Dynamical Properties. *J. Chem. Phys.* **1994**, *100*, 5106–5117.

(60) Cao, J.; Voth, G. A. The Formulation of Quantum Statistical Mechanics Based on the Feynman Path Centroid Density. III. Phase Space Formalism and Analysis of Centroid Molecular Dynamics. *J. Chem. Phys.* **1994**, *101*, 6157–6167.

(61) Cao, J.; Voth, G. A. The Formulation of Quantum Statistical Mechanics Based on the Feynman Path Centroid Density. IV. Algorithms for Centroid Molecular Dynamics. *J. Chem. Phys.* **1994**, *101*, 6168–6183.

(62) Cao, J.; Voth, G. A. The Formulation of Quantum Statistical Mechanics Based on the Feynman Path Centroid Density. V. Quantum Instantaneous Normal Mode Theory of Liquids. *J. Chem. Phys.* **1994**, *101*, 6184–6192.

(63) Hone, T. D.; Rossky, P. J.; Voth, G. A. A Comparative Study of Imaginary Time Path Integral Based Methods for Quantum Dynamics. *J. Chem. Phys.* **2006**, *124*, 154103.

(64) Leach, A. R. *Molecular Modelling Principles and Applications*, 2nd ed.; Pearson Education Limited, 2001.

(65) Kananenka, A. A.; Skinner, J. L. Fermi Resonance in OH-stretch Vibrational Spectroscopy of Liquid Water and the Water Hexamer. *J. Chem. Phys.* **2018**, *148*, 244107.

(66) Neese, F. The ORCA Program System. *WIREs Comput. Mol. Sci.* **2012**, *2*, 73–78.

(67) Towns, J.; Cockerill, T.; Dahan, M.; Foster, I.; Gaither, K.; Grimshaw, A.; Hazlewood, V.; Lathrop, S.; Lifka, D.; Peterson, G. D. et al. XSEDE: Accelerating Scientific Discovery. *Comput. Sci. Eng.* **2014**, *16*, 62–74.

TOC Figure